JACS
JOURNAL OF THE AMERICAN CHEMICAL SOCIETY
pubs.acs.org/JACS
Article

Flexible Phenanthracene Nanotubes for Explosive Detection

Simon C. Rickert,[⊥] Shao-Xiong Lennon Luo,[⊥] Joshua Bahr, Julia Kohn, Mantian Xue, Andreas Hansen, Stefan Grimme,* Stefan-S. Jester,* Timothy M. Swager,* and Sigurd Höger*

Cite This: *J. Am. Chem. Soc.* 2024, 146, 2986−2996
Read Online

ABSTRACT: Phenanthracene nanotubes with arylene-ethynylene-butadiynylene rims and phenanthracene walls are synthesized in a modular bottom-up approach. One of the rims carries hexadecyloxy side chains, mediating the affinity to highly oriented pyrolytic graphite. Molecular dynamics simulations show that the nanotubes are much more flexible than their structural formulas suggest: In $\mathbf{1}_2$, the phenanthracene units act as hinges that flip the two macrocycles relative to each other to one of two possible sites, as quantum mechanical models suggest and scanning tunneling microscopy investigations prove. Unexpectedly, both theory and experiment show for $\mathbf{1}_3$ that the three phenanthracene hinges are deflected from the upright position, accompanied by a deformation of both macrocycles from their idealized sturdy macroporous geometry. This flexibility together with their affinity to carbon-rich substrates allows for an efficient host−guest chemistry at the solid/gas interface opening the potential for applications in single-walled carbon nanotube-based sensing, and the applicability to build new sensors for the detection of 2,4,6-trinitrotoluene via nitroaromatic markers is shown.

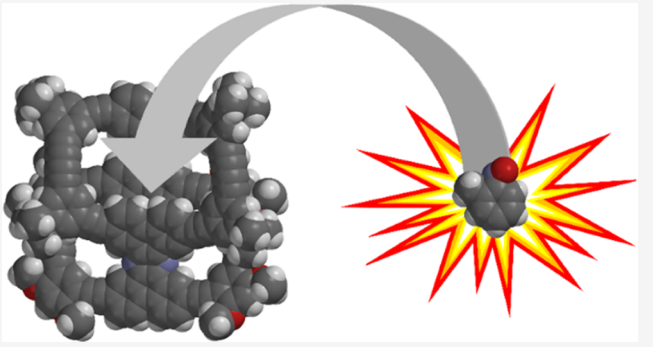

INTRODUCTION

The bottom-up synthesis of carbon nanobelts, which are cutouts of various carbon nanotubes, and their host−guest chemistry has been in the focus of intense research in recent years.[1−3] Similar to other tubular structures such as cyclodextrins, resorcinarene cavitands, or cucurbiturils,[4−7] they can then be used as a host to interact with various neutral guest molecules, e.g., via $\pi-\pi$-stacking interactions and dispersion forces. For example, cavitand-functionalized single-walled carbon nanotubes have been shown to selectively detect *N*-methylammonium chloride, and a porphyrin nanobelt has been shown to bind fullerenes.[8,9] Further applications of such selective host−guest interactions have been demonstrated in small molecule recognition and in membranes for efficient gas separation.[10−13] Other notable applications include use of heterogeneous catalysts by stabilizing intermediates in the cavity of these tubular supramolecules and the generation of porous organic polymers.[14−16] From the above examples, it is clear that nanotubular structures are indeed a relevant class of molecules with respect to host−guest chemistry in solution and on surfaces.

Apart from cyclodextrins (e.g., amino CDs) and cyclopeptides,[5,17−20] most tube-like structures based on aromatic backbones are symmetrical with respect to their rim size and functionality.[21−23] However, nanotubes with different functionalities at their rims would allow them to interact with a solid support specifically with one rim so that they can be deposited on a surface in an orientation-controlled manner. This preserves access to the cavity and offers the potential for the selective adsorption of complementary guest molecules at the solid/liquid or solid/gas interface. For example, perthiolated β-cyclodextrins on gold nanoparticles can act as drug pockets.[24,25]

Specifically, the phenanthracene nanotubes (PNTs) synthesized in this work present themselves as potential selectors for electron-deficient aromatics, which are markers for explosives—a paramount concern for national security.[26,27] We transduce the selective host−guest interactions to electrical readouts by incorporating them in single-walled carbon nanotube (SWCNT)-based chemiresistive sensors, which display high sensitivity at room temperature, low power and cost demands, compact size, and adaptability for device integration.[28−31] In this study, we demonstrate the utility of PNTs, when integrated into carbon nanotube-based chemiresistors, as an attractive alternative approach with simplicity, high sensitivity, selectivity, and robustness to achieve the real-time and continuous detection of explosives.

Regarding synthetic approaches toward tube- and belt-shaped nanostructures, various strategies have been developed

Received: July 28, 2023
Revised: January 8, 2024
Accepted: January 9, 2024
Published: January 23, 2024

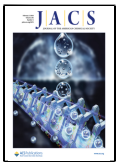

https://doi.org/10.1021/jacs.3c08131
J. Am. Chem. Soc. 2024, 146, 2986−2996

over the past years.[32−34] We have recently used H-shaped arylene-alkynylenes[35] as monomers for the synthesis of nanosized shape-persistent ladder oligomers and polymers.[36] Specifically, H-shaped ladder precursors are synthesized in a stepwise manner, where four rigid rod units are connected to a rung. Their ethynyl ends are protected with two silyl protective groups of different stability. After selective deprotection of the more labile pair of groups, a first strand is polymerized, and subsequent deprotection of the remaining protective groups allows for the ladder formation in an intramolecular zipping reaction. When the four linear rigid rods in H-shaped monomers are exchanged for kinked units, a selective deprotection of the first pair of ethynyl groups and subsequent homocoupling under ultrahigh dilution conditions should form a set of cyclooligomers (e.g., dimers and trimers, cf. Scheme 1)

Scheme 1. Synthesis of the Phenanthracene Nanotubes (Top: Cyclodimer 1_2; Bottom: Cyclotrimer 1_3; Schematically)

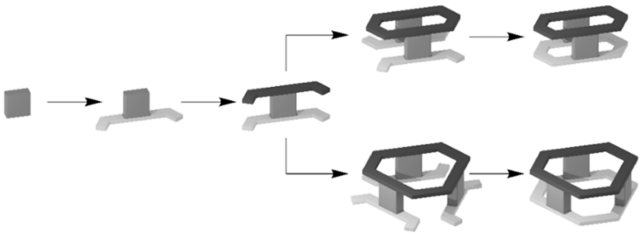

and polymers.[37−39] Separation of the shape-persistent macrocycles by recycling gel permeation chromatography (recGPC), followed by a second deprotection and homocoupling step, should lead to nanotubular structures with an internal cavity. Since the monomer synthesis is performed stepwise, both rims can differ in size and functionalization. Specifically, if one rim is more adsorptive to a given substrate, an orientation-controlled alignment of these nanostructures on the substrate should occur. The intrinsic nanotubular structure then enables host−guest chemistry at the solid−liquid or solid−gas interface in a sensing device.

RESULTS AND DISCUSSION

Herein, we present the synthesis of PNTs 1_2 and 1_3 with arylene-ethynylene-butadiynylene rims and phenanthracene walls (Figure 1) via a modular bottom-up approach. Theoretical models provide insight into the conformers formed upon interaction of the tubular species with graphene cutouts. The surface-mediated self-assembly on highly oriented pyrolytic graphite (HOPG) at the solution/solid interface is investigated by means of scanning tunneling microscopy (STM). Based on these results, both compounds were implemented in chemiresistive sensors for sensing of aromatic species, including nitroaromatics, aiming at the application as 2,4,6-trinitrotoluene (TNT) sensors.

Geometry. Molecular models of 1_2 and 1_3 are shown in Figure 2. The structures shown represent idealized sturdy macroporous geometries with fixed angles and bond lengths of the unfolded tubular structures. Alkoxy side chains were added with orientations of 90° for 1_2 and 60° for 1_3.

C_{2v} and C_{3v}-symmetric 1_2 and 1_3, respectively, consist of pairs of arylene ethynylene butadiynylene macrocycles that are connected by two and three phenanthracene units. The upper macrocycles of 1_2 and 1_3 carry four and six *t*-Bu groups, and the lower are substituted with eight and twelve $OC_{16}H_{33}$ groups, respectively.

Synthesis. The PNT target structures 1_2 and 1_3 can be viewed as nanotubular (cyclo-) oligomers of the (kinked) H-shaped monomer **11** (cf. Scheme 2). Their synthesis started with the selective deprotection of **2** under basic conditions to give **3** in 96% yield. The latter was coupled to phenanthrene diimine **4** under *Sonogashira* conditions to yield **5** in 62% yield. The central phenanthracene was then formed via a condensation of **5** with **6** in 92% yield, followed by another *Sonogashira* crosscoupling generating the second rim element of **10** in 67% yield. After quantitative deprotection under basic conditions, the monomer **11** was obtained as a neon yellow solid, which fluoresces upon irradiation in solution and the solid state (see Figures S6 and S7 in the Supporting Information). The usage of the (3-cyanopropyl)dimethylsilyl (CPDMS) protective group, a polar analogue of the trimethylsilyl (TMS) protective group, facilitated the column-chromatographic purification of **11** in the last step.[40] The latter was then (cyclo-) oligomerized by a Pd-catalyzed oxidative homocoupling (*Glaser* coupling) under high-dilution conditions, i.e., injection of the monomer into the catalyst solution over 24 h. RecGPC allowed an efficient separation of cyclodimer 12_2 and -trimer 12_3 from the crude product in yields of 31% and 9%, respectively. The absence of any terminal acetylene signals in the ^{1}H NMR spectra indicated the formation of cyclic structures. This is also supported by the limited set of signals, as expected for highly symmetrical cyclic molecules. Deprotection using TBAF yielded 13_2 and 13_3, which were treated without further purification under Pd-catalyzed oxidative homocoupling conditions. From the crude product mixture, 1_2 and 1_3 could be isolated by recGPC in 25 and 7% yields over two steps, respectively. Due to their symmetry and signal broadening in the aromatic region, a distinction via NMR spectroscopy was not possible. However, no residual terminal acetylene signals were visible in the ^{1}H NMR spectra, and the DOSY-NMR obtained for 1_2 only showed one distinct species indicating the full closure of all butadiyne-links (see Supporting Information (SI)). Also, ultraviolet/visible (UV/vis) and fluorescence spectra of 1_2 and 1_3 are alike since the length of the largest chromophore is unaltered upon oligomerization due to the meta substitution at the compound corners (see Figures S5 and S6).[41] However, the final products could gratifyingly be characterized and distinguished via analytical GPC and high-resolution MALDI-(+) mass spectrometry (see Figures S4, S44, S45, S49, and S50). Repeated synthesis on a small scale yielded total amounts of 29 mg of 1_2 and 7 mg 1_3.

The protection of the carbonyl units of the phenanthrene quinone is one of the critical steps in the reaction sequence. The imine protective group in **4** is necessary due to the often observed low yields when performing *Sonogashira* cross-couplings with phenanthrenequinones and related compounds.[42,43] It increases the compound solubility and decreases the ability of 1,2-diketone to deactivate the Pd species, most probably via complexation. Without protection, the coupling reaction gave irreproducible yields of only about 15%. Other strategies to overcome this issue include the protection as ketal.[44−46] However, the advantage of the imines is that they are inherently very labile toward acids. Therefore, they are already cleaved during aqueous workup and do not require an additional deprotection step.

https://doi.org/10.1021/jacs.3c08131
J. Am. Chem. Soc. 2024, 146, 2986−2996

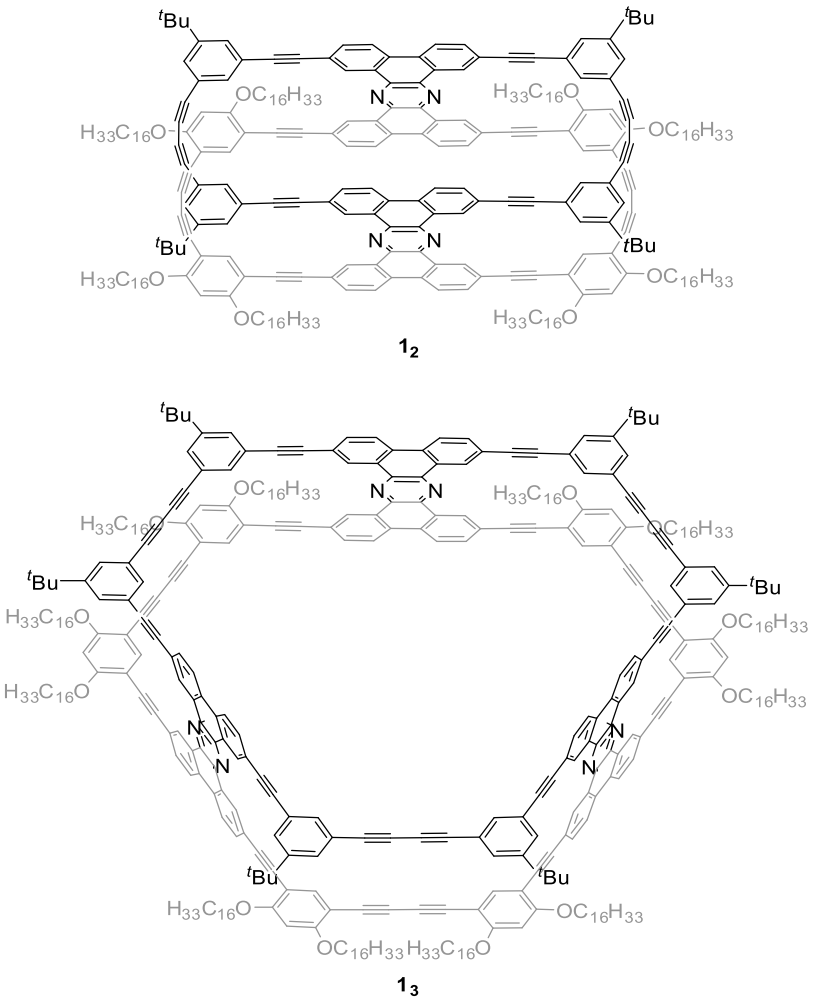

Figure 1. Chemical structures of the PNTs $\mathbf{1_2}$ and $\mathbf{1_3}$, implementing arylene-ethynylene-butadiynylene rims and phenanthracene walls. The *t*-Bu and $OC_{16}H_{33}$ substituents mediate compound solubility, whereas the latter also provide an affinity to HOPG for STM imaging.

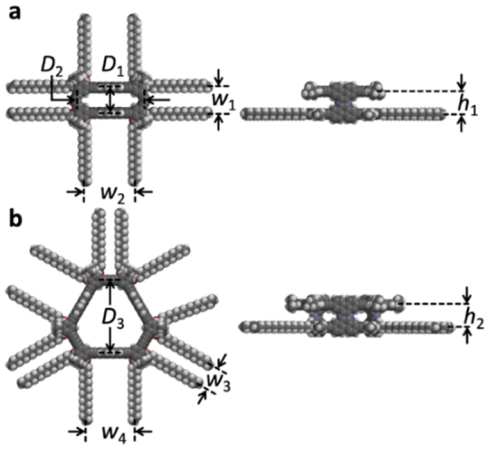

Figure 2. Top and side views of molecular models of (a) $\mathbf{1_2}$ and (b) $\mathbf{1_3}$; D_1 = 2.4 nm; D_2 = 0.8 nm; h_1 = 0.7 nm; w_1 = 0.9 nm; w_2 = 1.6 nm; D_3 = 2.4 nm^2; h_2 = 0.7 nm; w_3 = 0.8 nm; w_4 = 1.6 nm.

Molecular Modeling. We carried out computational studies and molecular dynamics (MD) at the tight-binding quantum chemistry level GFN2-xTB[47,48] with implicit solvation, conducted with the xtb 6.5.1 program package,[49] to assess on the one hand the conformations of $\mathbf{1_2}$ and $\mathbf{1_3}$ after adsorption on graphene, a model substrate for HOPG used in the STM experiments, and on the other hand the flexibility of $\mathbf{1_2}$ and $\mathbf{1_3}$ in solution. While the alkyl side chains are known to mediate adsorption to both substrates, they should not affect the conformation of the tubular structures of $\mathbf{1_2}$ and $\mathbf{1_3}$ and are therefore neglected here. The orientation-controlled adsorption of both species should nominally generate molecular cavities on the surface, accessible from above.

However, $\mathbf{1_2}$ (Figure 3a) adopts a more compressed conformation in which the phenanthracene units act as "hinges". One of the latter (arrow 1 in Figure 3a) is oriented in parallel to the HOPG substrate, while the other (arrow 2) is tilted and partly overlaps with the first. This leads to an offset of the upper macrocycle (arrow 3) relative to the lower one (arrow 4) and a slightly nonplanar geometry of the upper ring. The collapse of the tubular structure is possible due to rotation of both phenanthracene hinges in parallel. Based on a model with fixed angles and bond lengths, we expected that the phenanthracene units in $\mathbf{1_3}$ are (due to C_{3v} symmetry) not aligned in parallel. Therefore, they cannot flip in different directions but block each other. This should consequently lead to a three-dimensional shape, in which both (bottom and top) shape-persistent macrocyclic rims of the tube would adopt a certain distance, such as providing an intramolecular cavity (e.g., filled with solvent molecules or analytes). Contrary to this assumption, the lower macrocycle in $\mathbf{1_3}$ (arrow 5 in Figure

https://doi.org/10.1021/jacs.3c08131
J. Am. Chem. Soc. 2024, 146, 2986−2996

Scheme 2. Synthetic Approach Towards H-Shaped Monomer 11 and the Desired Nanotubular Target Structures 1_2 and 1_3.[a]

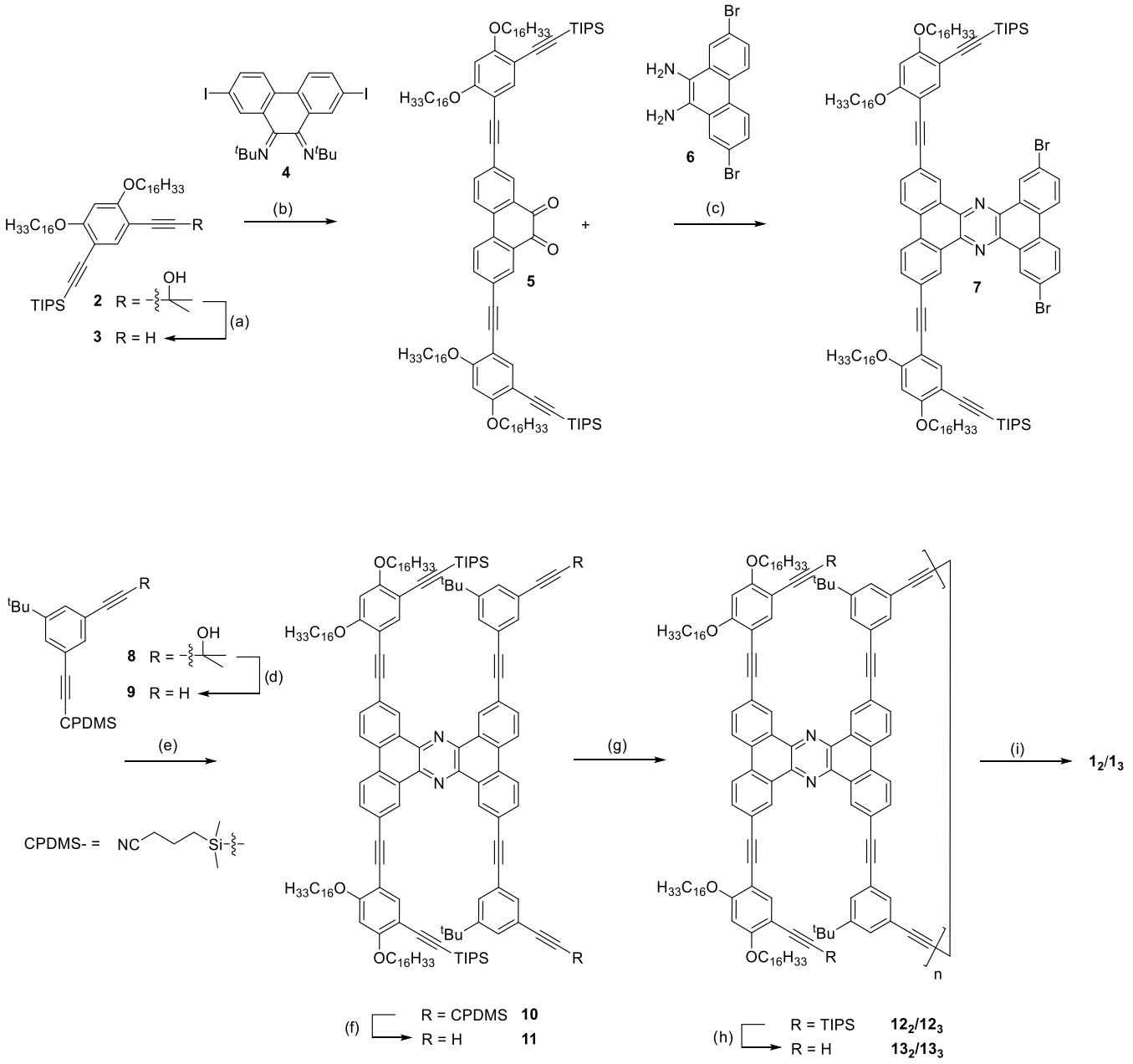

[a]Reagents and Conditions: (a) NaOH, toluene, reflux, 1 h, 96%; (b) $PdCl_2(PPh_3)_2$ (cat.), PPh_3, CuI (cat.), piperidine:THF (2:1), 40 °C, 20 h, 62%; (c) $CHCl_3$, AcOH, reflux, 24 h, 92%; (d) NaOH (dry), toluene, reflux, 30 min, 61%; (e) $Pd(OAc)_2$ (cat.), *XPhos*, CuI (cat.), piperidine:THF (2:1), 80 °C, 20 h, 67%; (f) K_2CO_3 (anhydr.), MeOH:THF (1:2), r.t., 24 h, >99%; (g) $PdCl_2(PPh_3)_2$ (cat.), CuI (cat.), I_2, THF:DIPA (1:1), 50 °C, injection over 24 h, 31% $\mathbf{12_2}$ and 9% $\mathbf{12_3}$; (h) TBAF (1 M in THF), THF, 35 °C, 3 h; (i) $PdCl_2(PPh_3)_2$ (cat.), CuI (cat.), I_2, THF:DIPA (1:1), 50 °C, injection over 48 h, 25% $\mathbf{1_2}$ and 7% $\mathbf{1_3}$, over two steps respectively.

3b) retains its ideal geometry (resembling a triangular shape), and the structure collapses by the upper macrocycle (arrow 6) being compressed at one end, adopting a "bicycle saddle" shape. MDs additionally show that the idealized sturdy macroporous forms are conformationally stable neither when adsorbed on the surface nor when free in solution, and instead, $\mathbf{1_2}$ and $\mathbf{1_3}$ prefer a maximalization of the $\pi-\pi$-stacking interactions, which is achieved by the aforementioned collapsing of the hinges. Note that the MDs only consider a single molecule of $\mathbf{1_2}$ or $\mathbf{1_3}$, respectively, and in this aspect, do not reflect the STM experiments, as there the bottom macrocycles are immobilized in a two-dimensional (2D) crystal. Additionally, $\mathbf{1_3}$ is not able to collapse all three hinges at the same time rendering it a bit sturdier than $\mathbf{1_2}$, but still far away from rigidity in general or real shape persistence. Nevertheless, the PNTs are more rigid than their SPM analogues, as shown by the means of MD simulations and the distance distribution analysis of opposing condensed aromatic units of the rim (cf., Figure S2).

This is only possible due to the flexibility (or elasticity) of the nominally shape-persistent constituents,[50] particularly the diacetylenes.[51−54] Moreover, the phenanthracene units in $\mathbf{1_3}$ do not overlap (as in $\mathbf{1_2}$) but lie flat on the graphene, resulting in a wavelike structure of the upper ring and two crossings of

https://doi.org/10.1021/jacs.3c08131
J. Am. Chem. Soc. 2024, 146, 2986−2996

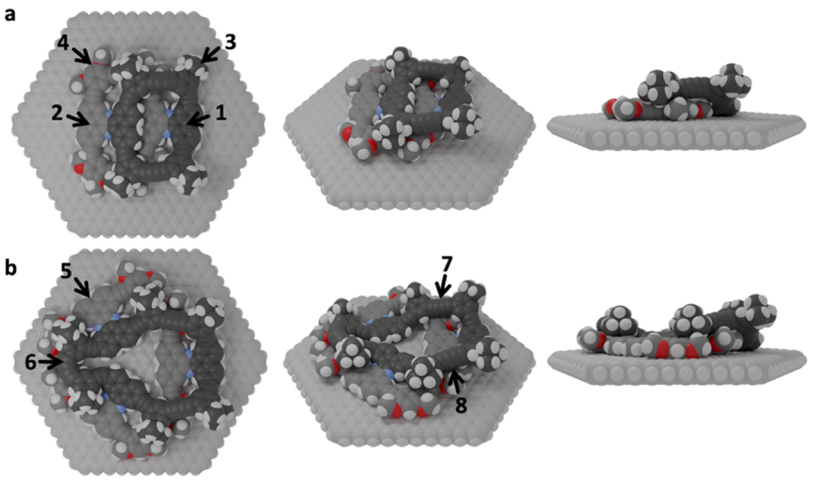

Figure 3. Top, perspective, and side views of (a) $\mathbf{1}_2$ and (b) $\mathbf{1}_3$ on a graphene cutout optimized at the GFN2-xTB level of theory (with hexadecyloxy side chains omitted and graphene cut to $C_{600}H_{60}$ for clarity, cf. SI). Arrows 1 and 2 indicate phenanthracene units aligned in parallel to the surface and tilted, respectively; arrows 3/6 and 4/5 indicate the lower and upper macrocycles, respectively; and arrows 7 and 8 indicate crossings of the upper and lower macrocycles.

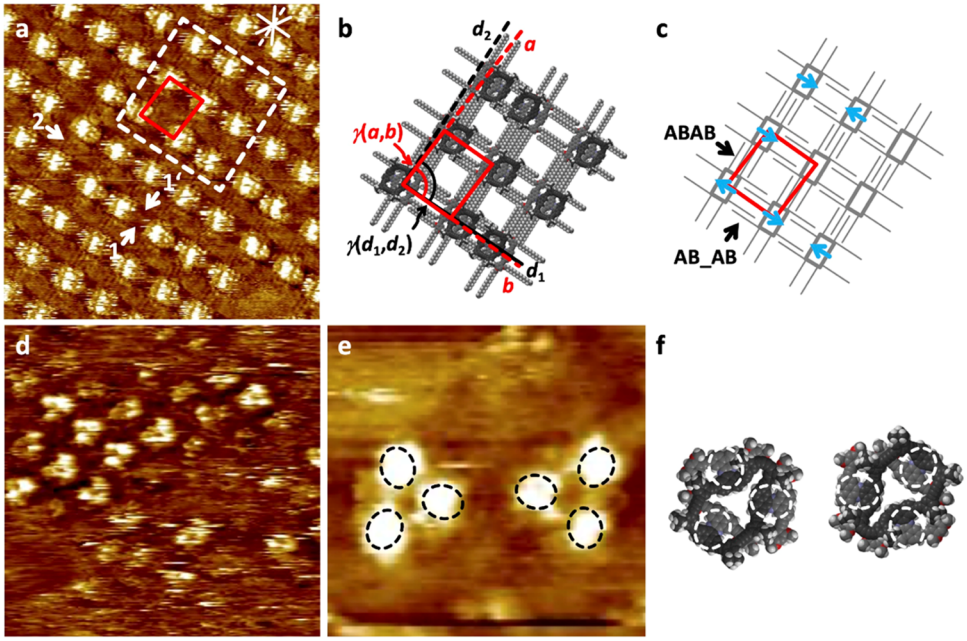

Figure 4. (a, d, e) Scanning tunneling microscopy images, (b) proposed supramolecular model, (c) schematic model of the bottom rim, and (f) molecular models (neglecting the side chains) of (a–c) a self-assembled monolayer of $\mathbf{1}_2$ and (d–f) $\mathbf{1}_3$ at the solution/solid interface of the respective compound in 1,2,4-trichlorobenzene and highly oriented pyrolytic graphite. Image and unit cell parameters: (a) $\mathbf{1}_2$: $c = 5 \times 10^{-6}$ M, 30×30 nm^2, $V_S = -1.3$ V, $I_t = 23$ pA; $a = (4.3 \pm 0.2)$ nm, $b = (3.7 \pm 0.2)$ nm, $\gamma(a,b) = (87 \pm 2)°$, $\gamma(b,d_1) = (1 \pm 2)°$, $\gamma(d_1,d_2) = (90 \pm 4)°$; (d) $\mathbf{1}_3$: $c = 3 \times 10^{-5}$ M, 40×40 nm^2 (internal scanner calibration), $V_S = -0.7$ V, $I_t = 18$ pA; (e) $\mathbf{1}_3$: $c = 3 \times 10^{-5}$ M, 9.4×9.4 nm^2 (internal scanner calibration), $V_S = -0.7$ V, $I_t = 20$ pA; all samples thermally annealed for 20 s at 80 °C. Red lines in panels (a–c) indicate the unit cell; white and black solid (and dashed) lines in panels (a, b) indicate the HOPG main axis (and armchair) directions; gray boxes and lines in panel (c) indicate the bottom rims and interdigitation pattern of the hexadecyloxy side chains; blue arrows in panel (c) indicate the tilting directions of 6 out of 9 top rims in the marked surface region in panel (a); black and white dashed ovals in panels (e, f) highlight the phenanthracene units.

the upper and lower macrocycles (arrows 7 and 8, respectively).

STM Studies. We aimed to study the adsorption behavior of $\mathbf{1}_2$ and $\mathbf{1}_3$ on a carbon-based substrate related to the nanotubular environment of later sensing experiments. Therefore, in situ STM studies were conducted at the solid/liquid interface of HOPG and a dilute solution of the respective compound in a suitable solvent, i.e., 1,2,4-trichlorobenzene (TCB).

$\mathbf{1}_2$ forms a self-assembled monolayer (SAM) in which a periodic, checkerboard-like pattern is observed in the STM image (Figure 4a). Each brightly appearing surface region (that corresponds to an aromatic backbone) is surrounded by regions with darker image contrast attributed to regions covered with the aliphatic (alkoxy chain) periphery.[55] This gives a first indication that all molecules of $\mathbf{1}_2$ are oriented with the alkoxy-substituted tube rim toward the HOPG substrate, as intended. Along one direction (denoted as unit cell vector b), each pair of adjacent aromatic backbones interacts via four side

https://doi.org/10.1021/jacs.3c08131
J. Am. Chem. Soc. 2024, 146, 2986–2996

chains that align with one of the three HOPG main axis directions (denoted as d_1),[56−60] and appear as the regions of darkest contrast within the STM image (e.g., arrows 1 and 1′ in Figure 4a). More precisely, these four chains assemble in two pairs of chains that are aligned in an antiparallel direction (with an intermediate gap), which can be viewed as a "widened" interdigitation pattern (AB_AB packing; cf. Figure 4c). The other four of the eight total chains of each molecule are also clearly observable (as linear contrast variations of medium brightness, e.g., arrow 2 in Figure 4a) and mediate the interaction of two adjacent backbones along the direction denoted as *a*. Unexpectedly, they do not follow one of the main axis (or *zigzag*) directions of the underlying HOPG substrate but instead are aligned orthogonal to the previously discussed chain direction. This arrangement along the *armchair* direction of graphite (denoted as d_2 in Figure 4b)—while rare—has previously been observed for (cyclo-) alkanes and alkyl chains in sterically constrained environments. Examples include rotated quadratic domains (where the domain width is identical to the length of a molecule or multiples thereof)[61−63] and alkoxy chains in a pocket between rigid aromatic backbones (where the majority of other side chains is aligned along the main axis).[64] To this two-dimensional (2D) crystalline pattern, a (nearly rectangular) unit cell with parameters $a = (4.3 \pm 0.2)$ nm, $b = (3.7 \pm 0.2)$ nm, and $\gamma(a,b) = (87 \pm 2)°$ rotated relative to d_1 with $\gamma(b,d_1) = (1 \pm 2)°$ is indexed. Note that the tube rim carrying the eight hexadecyloxy side chains is in close contact with the substrate and acts as a two-dimensional "anchor", mounted in a fixed lateral position on the HOPG substrate, as dictated by the periodic alkoxy chain periphery and schematically indicated by the gray boxes and lines in Figure 4c. The other tube rim, carrying four *t*-butyl groups, should in principle flip to either side (cf. Figure 3a). While the regions of brighter contrast in the image are not resolved clearly enough to point out specific details of the upper and lower rims, a notable distinction in the position of the brightest contrast feature is made when visually comparing adjacent molecules. In the STM image shown in Figure 4a, we could clearly identify that out of 55 molecules, 22 adopt the conformation oriented to the top left (of the STM image shown) and 16 are tilted to the bottom-right (cf. SI and blue arrows in Figure 4c). Therefore, the upper rims are in close contact with the lower rims after having flipped randomly to either side during the adsorption process and then stay in this orientation throughout the STM measurement. Consequently, the cavity of the PNTs is rather compressed and adaptable in size, allowing for selectivity in the host−guest interactions of later sensing experiments.

Monolayers of $\mathbf{1}_3$ have also been observed under similar conditions via STM (Figure 4d,e). However, the tendency to form regular 2D patterns is far less pronounced, and only small regions of the surface show ordered patterns (Figure 4d) where rows of triangles that point in opposite directions alternate. Figure 4e and f shows two molecules of $\mathbf{1}_3$ on the HOPG surface. Three bright contrast features per molecule are clearly attributed to the phenanthracene units (due to their electronic conductivity when in contact with the HOPG substrate) and are surrounded by darker regions attributed to the alkoxy chain periphery. The parts of the backbone to which alkoxy chains are attached are again assumed to be closest to the surface. As no highly ordered domain over a large surface area (such as for $\mathbf{1}_2$) has been observed, the exact positions of the alkoxy chains remain largely unresolved.

Explosive Detection. Based on these structural investigations, it was envisioned that the PNTs would deposit on a carbon-based substrate to serve as selectors in a chemiresistive device. Preliminary studies used a quartz crystal microbalance (QCMB), and a diluted solution of $\mathbf{1}_2$ was drop-casted on gold-coated QCM electrodes. These investigations revealed reversible adsorption and desorption of aromatic molecules from the gas phase, and the flexible nature of $\mathbf{1}_2$ provides for selectivity between different aromatic analytes (Figure 5a).

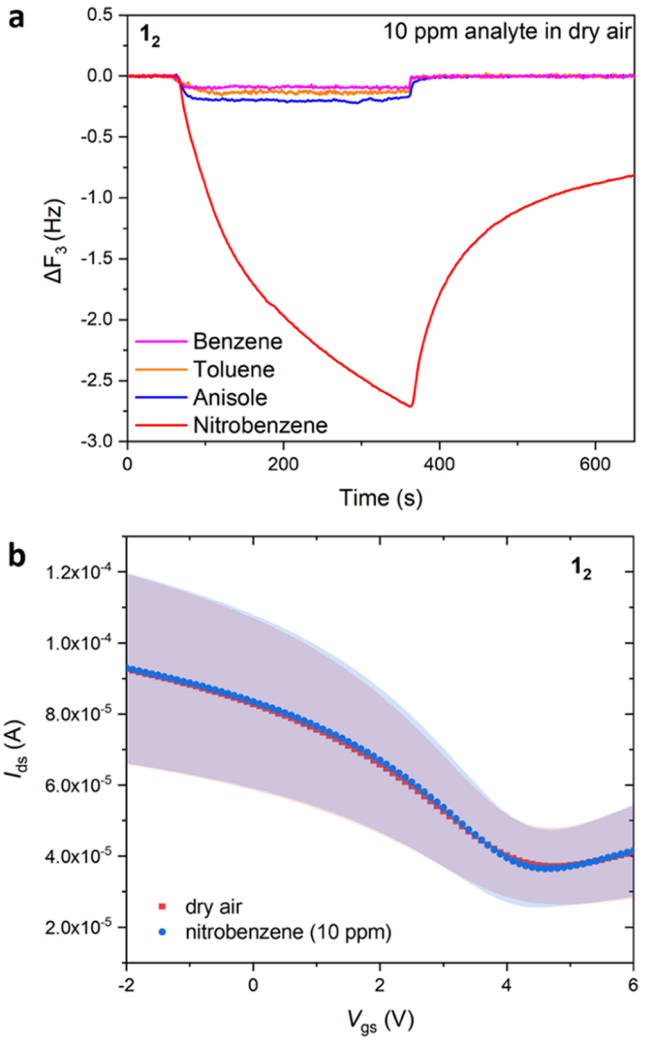

Figure 5. (a) Quartz crystal microbalance measurements with dimer $\mathbf{1}_2$ for different analytes (10 ppm in dry air); depicted is the change in the third harmonic of the resonant frequency with time upon analyte exposure; (b) current−voltage (I−V) characteristics of graphene-based field-effect transistors (GFETs) with $\mathbf{1}_2$ before and after 5 min exposure of 10 ppm of nitrobenzene in dry air. ($N \geq 16$).

However, when $\mathbf{1}_2$ was used in graphene-based field-effect transistors (GFETs), no significant change was observed in the transfer characteristics of the GFETs upon exposure to the same analytes (Figure 5b). This indicated that the incorporation of a guest molecule in the PNTs did not have a significant effect on the electronic interaction between the PNT and the graphene that would ultimately change the conductance of the GFETs.[65]

Therefore, chemiresistive devices based on a network of PNT-functionalized single-walled carbon nanotubes

https://doi.org/10.1021/jacs.3c08131
J. Am. Chem. Soc. 2024, 146, 2986−2996

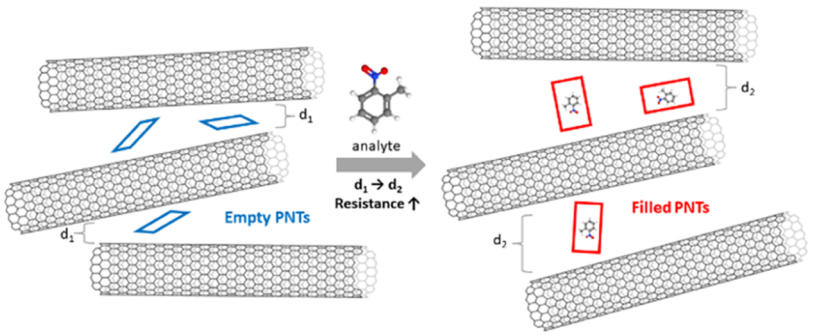

Figure 6. Illustration of a swelling-based sensing mechanism, showing the expansion of the SWCNT network ($d_2 > d_1$) upon the binding of nitrotoluene to the PNTs.

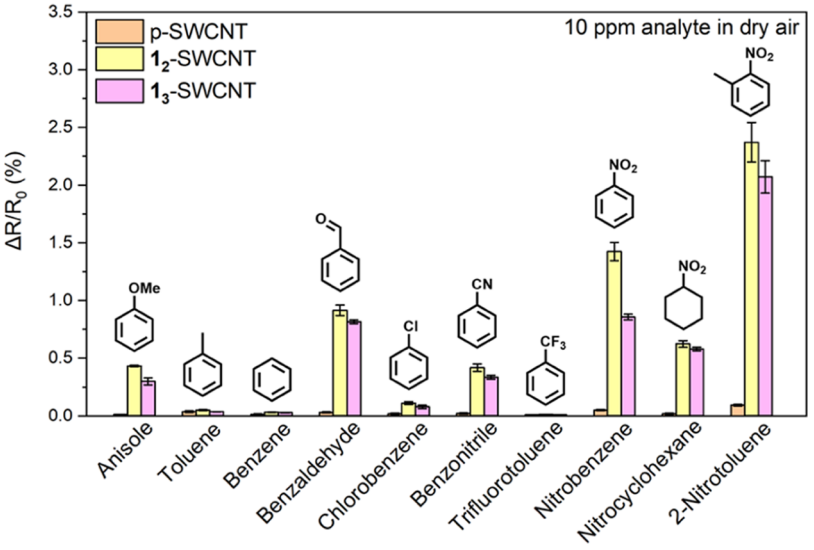

Figure 7. Chemiresistive responses of $\mathbf{1}_2$-SWCNT (yellow), $\mathbf{1}_3$-SWCNT (pink), and p-SWCNT (orange) upon exposure to 10 ppm of various analytes in dry air for 5 min. ($N \geq 4$).

(SWCNTs) were fabricated and tested.[28] In particular, SWCNTs (0.1 mg/mL) are dispersed in an *ortho*-dichlorobenzene solution of PNTs (1 mg/mL) using ultrasonication. Subsequently, the resulting dispersion (1 μL) is drop-cast between gold electrodes on a glass substrate to form the chemiresistor devices. The operating mechanism of SWCNT-based chemiresistors does not rely exclusively on a change in the electronic interaction between SWCNTs and the selector (PNTs). In these devices, a response can be generated by modulating the number of interconnection points of conduction pathways in the SWCNT network. The number of interconnections is reduced by the swelling of the SWCNT network induced by interactions of the PNT selectors with an analyte.[66,67] We expect that $\mathbf{1}_2$ will behave as a molecular actuator triggered by the binding of an analyte to separate SWCNTs based upon its compressed guest-free structure as previously described (Figure 6).

Indeed, this way, it was possible to replicate the signals observed upon exposure to aromatic analytes when using the QCMB, as well as their relative signal strength (Figure 7). This shows that the selectivity is transferred from the PNTs to the SWCNT-based chemiresistors, and that these PNTs can be used effectively as selectors. Further studies using $\mathbf{1}_2$ ($\mathbf{1}_2$-SWCNT) showed clear selectivity toward nitrotoluene, whereas pristine SWCNTs (p-SWCNT) showed no selectivity whatsoever. Using $\mathbf{1}_3$ ($\mathbf{1}_3$-SWCNT), the same selectivity as for $\mathbf{1}_2$-SWCNT was observed but less pronounced, which can be attributed to the larger cavity size. This supports the proposed swelling mechanism as mode of detection for the sensor. To enable this mechanism, PNTs had to be incorporated into the SWCNT network, by forming a dispersion in *o*-dichlorobenzene (*o*-DCB) via ultrasonication, rather than simply depositing the PNTs on top of the SWCNT network. Sensor signals were only observed from the codeposition from the PNT-SWCNT dispersion, because for the swelling of the PNTs to be able to break the interconnections between SWCNTs, the PNTs must have a strong interaction with the SWCNT network. This interaction could be detected by Raman spectroscopy. Shifts of the SWCNT $C(sp^2)$-$C(sp^2)$ stretching mode (G band) to lower wavenumbers were observed in $\mathbf{1}_2$-SWCNT and $\mathbf{1}_3$-SWCNT, compared to the pristine SWCNTs (cf. Figure S13). Thus, these results indicate a strong interaction via an *n*-type doping influence from the PNTs to the intrinsically *p*-doped SWCNTs.[68] The monomer **11** itself did not show any enhanced selectivity compared to the pristine SWCNTs, indicating the need for a cavity (cf. Figure S14). Moreover, monomer **11** dispersed the SWCNTs poorly compared to $\mathbf{1}_2$ and $\mathbf{1}_3$, leading to phase-separated aggregates.

The observed selectivity of the chemiresistor does not directly correlate with the electronic structure of the aromatic analytes (Figure 7). Furthermore, the nitro-group is not the

https://doi.org/10.1021/jacs.3c08131
J. Am. Chem. Soc. 2024, 146, 2986−2996

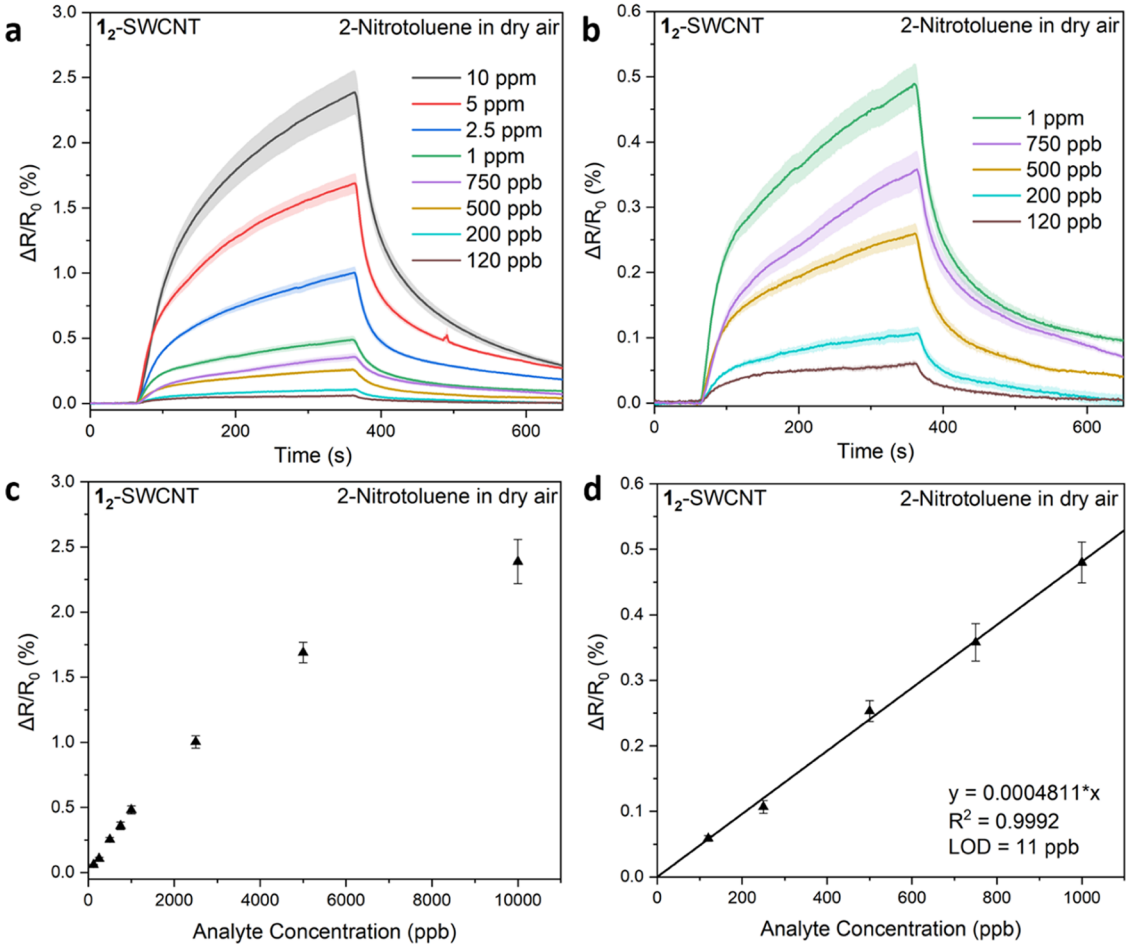

Figure 8. Chemiresistive response-traces and sensor response to analyte concentration relationship for $\mathbf{1}_2$-SWCNT chemiresistors upon exposure to 2-nitrotoluene in dry air in different concentrations (a, c) below 1 ppm (b, d). ($N \geq 4$).

primary selectivity factor either, as the nonaromatic counterpart nitrocyclohexane gave significantly lower signal responses. In addition, analytes with a higher boiling and melting point adsorb more easily onto surfaces; however, no significant correlation was observed. It can be concluded that a multicomponent sensing mechanism involving an interaction of the aromatic system and the electron-withdrawing nitro-group with the respective PNTs $\mathbf{1}_2$ or $\mathbf{1}_3$ led to the observed selectivity toward nitroaromatic analytes. This interaction itself can be surmised to be based on a differentially efficient induced-fit of the PNT hosts toward the respective analyte guest molecules.

In the context of good selectivity of PNT-based chemiresistors toward nitroaromatic analytes, we probe their potential to detect low concentrations of 2-nitrotoluene as a marker for TNT and thus contribute to the development of new lightweight, portable, and solution-processable explosive sensors. 2-Nitrotoluene is a good marker for TNT because it is always present in explosive-grade TNT samples, which have a low vapor pressure (<5 ppb) at room temperature.[69] Therefore, we evaluate the signal responses toward different concentrations of 2-nitrotoluene and its signal strength can be correlated to vapor. Only when the concentration of 2-nitrotoluene is below 1 ppm could a linear dependency be observed, which may be explained by a saturation of the sensor with the analyte at higher concentrations. Using only analyte concentrations below 1 ppm reveals a highly linear correlation between the sensor response and analyte concentration (Figure 8). This linear correlation was then used to determine the calculated limit of detection (LOD; cf. SI), which amounted to 11 ppb.[70]

Comparing the LOD of the sensors manufactured in this work with other carbon nanotube-based chemiresistors, the low ppb-level sensitivity is among the best results published to this date.[71−76] Lower LODs have been obtained for solution sensing, but the utility of these devices in the detection of explosives is not operationally useful because they cannot detect solid explosives by direct vapor detection.[77] Other sensing methods which are based on chromatography or fluorescence quenching, rather than a chemiresistive response, give LODs two orders of magnitude lower, i.e., in the range of few ppq.[69,78] However, they require larger devices and are more costly to manufacture. The low power and inexpensive nature of chemiresistors allows for deployment of badges into workclothing for hazardous environments or in arrays for distributed (large area) monitoring.

To ensure reliable signals from the sensor, not only the selectivity with respect to similar compounds was tested but also interference from volatile organic compounds (VOCs). These VOCs have low boiling points and could give false positive signal responses when being present in larger quantities than the 2-nitrotoluene to be detected.

Experiments showed that even ten times higher concentrations of VOCs gave only a fraction of the signal response

https://doi.org/10.1021/jacs.3c08131
J. Am. Chem. Soc. 2024, 146, 2986−2996

observed for 2-nitrotoluene (cf. Figure S17), comparable to the signal of sensors using pristine SWCNTs. Regarding the influence of humidity on the sensing capability of the chemiresistor, it was found that there was no significant lowering of the signal response when the relative humidity was increased from 0 to 70% (cf., Figure S16). Furthermore, the sensors show good long-term stability under ambient storage conditions, retaining more than 70% of the initial signal responses toward 2-nitrotoluene after 30 days (cf. Figure S18).

CONCLUSIONS

We have reported the modular synthesis of PNTs in which both rims of the tube contain different side groups. Specifically, *t*-butyl groups and hexadecyloxy groups at either rim give an orientation control when the compounds are physisorbed on HOPG due to the high tendency of long alkyl chains to align on the graphite. The 2D adsorbates were investigated by means of STM and the images, together with quantum chemical calculations, show that the molecules are much more flexible than their structural formulas suggest. This dynamic structural feature allows these materials to behave as dynamic actuators triggered by analyte binding. By deploying our molecular nanotubes as in a random SWCNT nanowire matrix, we can modulate the SWCNT−SWCNT contacts with analyte adsorption to create strong selective sensory responses with parts per billion detection limits of a TNT marker. In this way, a new potent chemiresistive sensor for explosive detection is demonstrated with high sensitivity, selectivity, and durability.

ASSOCIATED CONTENT

Supporting Information

The Supporting Information is available free of charge at https://pubs.acs.org/doi/10.1021/jacs.3c08131.

Synthesis, additional STM images, computational details and structure coordinates, additional sensing experiments (PDF)
[1]2_on_graphene_sheet (XYZ)
[1]3_on_graphene_sheet (XYZ)
(1)2_in_solution_MD (MP4)
(1)2_on_graphene_MD (MP4)
(1)3_in_solution_MD (MP4)
(1)3_on_graphene_MD (MP4)
(M1)2_in_solution_MD (MP4)
(M1)2_on_graphene_MD (MP4)
(M1)3_in_solution_MD (MP4)
(M1)3_on_graphene_MD (MP4)

AUTHOR INFORMATION

Corresponding Authors

Stefan Grimme − *Mulliken Center for Theoretical Chemistry, University of Bonn, 53115 Bonn, Germany;* orcid.org/0000-0002-5844-4371; Email: grimme@thch.uni-bonn.de

Stefan-S. Jester − *Kekulé-Institut für Organische Chemie und Biochemie der Universität Bonn, 53121 Bonn, Germany;* orcid.org/0000-0003-3093-4368; Email: stefan.jester@uni-bonn.de

Timothy M. Swager − *Department of Chemistry and Institute for Soldier Nanotechnologies, Massachusetts Institute of Technology, Cambridge, Massachusetts 02139, United States;* orcid.org/0000-0002-3577-0510; Email: tswager@mit.edu

Sigurd Höger − *Kekulé-Institut für Organische Chemie und Biochemie der Universität Bonn, 53121 Bonn, Germany;* orcid.org/0000-0001-9987-0185; Email: hoeger@uni-bonn.de

Authors

Simon C. Rickert − *Kekulé-Institut für Organische Chemie und Biochemie der Universität Bonn, 53121 Bonn, Germany;* orcid.org/0009-0000-5575-8482

Shao-Xiong Lennon Luo − *Department of Chemistry and Institute for Soldier Nanotechnologies, Massachusetts Institute of Technology, Cambridge, Massachusetts 02139, United States;* orcid.org/0000-0001-5308-4576

Joshua Bahr − *Kekulé-Institut für Organische Chemie und Biochemie der Universität Bonn, 53121 Bonn, Germany*

Julia Kohn − *Mulliken Center for Theoretical Chemistry, University of Bonn, 53115 Bonn, Germany*

Mantian Xue − *Department of Electrical Engineering & Computer Science, Massachusetts Institute of Technology, Cambridge, Massachusetts 02139, United States*

Andreas Hansen − *Mulliken Center for Theoretical Chemistry, University of Bonn, 53115 Bonn, Germany;* orcid.org/0000-0003-1659-8206

Complete contact information is available at: https://pubs.acs.org/10.1021/jacs.3c08131

Author Contributions

⊥S.C.R. and S.-X.L.L. contributed equally to this work. The manuscript was written through contributions of all authors./ All authors have given approval to the final version of the manuscript.

Notes

The authors declare no competing financial interest.

ACKNOWLEDGMENTS

The authors gratefully acknowledge support from the Deutsche Forschungsgemeinschaft (DFG, RTG-2591 "Template-designed Organic Electronics−TIDE" and Project-ID 455731873) and the National Science Foundation (DMR-2207299).

ABBREVIATIONS

DIPA, (diisopropyl)amine; THF, tetrahydrofuran; TBAF, tetrabutylammonium fluoride; *Xphos*, dicyclohexyl[2′,4′,6′-tris(propan-2-yl)[1,1′-biphenyl]-2-yl]phosphane

REFERENCES

(1) Cheung, K. Y.; Watanabe, K.; Segawa, Y.; Itami, K. Synthesis of a zigzag carbon nanobelt. *Nat. Chem.* **2021**, *13* (3), 255−259.
(2) Sun, Z.; Ikemoto, K.; Fukunaga, T. M.; Koretsune, T.; Arita, R.; Sato, S.; Isobe, H. Finite phenine nanotubes with periodic vacancy defects. *Science* **2019**, *363* (6423), 151−155.
(3) Xia, Z.; Pun, S. H.; Chen, H.; Miao, Q. Synthesis of Zigzag Carbon Nanobelts through Scholl Reactions. *Angew. Chem., Int. Ed.* **2021**, *60* (18), 10311−10318.
(4) Assaf, K. I.; Nau, W. M. Cucurbiturils: from synthesis to high-affinity binding and catalysis. *Chem. Soc. Rev.* **2015**, *44* (2), 394−418.
(5) Crini, G. Review: A History of Cyclodextrins. *Chem. Rev.* **2014**, *114* (21), 10940−10975.
(6) Pinalli, R.; Suman, M.; Dalcanale, E. Cavitands at Work: From Molecular Recognition to Supramolecular Sensors. *Eur. J. Org. Chem.* **2004**, *2004* (3), 451−462.
(7) Timmerman, P.; Verboom, W.; Reinhoudt, D. N. Resorcinarenes. *Tetrahedron* **1996**, *52* (8), 2663−2704.

(8) Dionisio, M.; Schnorr, J. M.; Michaelis, V. K.; Griffin, R. G.; Swager, T. M.; Dalcanale, E. Cavitand-functionalized SWCNTs for N-methylammonium detection. *J. Am. Chem. Soc.* **2012**, *134* (15), 6540−6543.
(9) Xue, S.; Kuzuhara, D.; Aratani, N.; Yamada, H. Synthesis of a Porphyrin(2.1.2.1) Nanobelt and Its Ability To Bind Fullerene. *Org. Lett.* **2019**, *21* (7), 2069−2072.
(10) Wu, J.; Liang, C. Z.; Naderi, A.; Chung, T.-S. Tunable Supramolecular Cavities Molecularly Homogenized in Polymer Membranes for Ultraefficient Precombustion CO2 Capture. *Adv. Mater.* **2022**, *34* (3), No. 2105156.
(11) Kong, L.; Wang, J.; Meng, F.; Chen, X.; Jin, Z.; Li, M.; Liu, J.; Huang, X.-J. Novel hybridized SWCNT−PCD: synthesis and host−guest inclusion for electrical sensing recognition of persistent organic pollutants. *J. Mater. Chem.* **2011**, *21* (30), 11109−11115, DOI: 10.1039/c0jm04552g.
(12) Ogoshi, T.; Ikeya, M.; Yamagishi, T.; Nakamoto, Y.; Harada, A. Enhancement of Water Solubility of Single-Walled Carbon Nanotubes by Formation of Host−Guest Complexes of Cyclodextrins with Various Guest Molecules. *J. Phys. Chem. C* **2008**, *112* (34), 13079−13083.
(13) Wang, F.; Yang, Y.; Swager, T. M. Molecular Recognition for High Selectivity in Carbon Nanotube/Polythiophene Chemiresistors. *Angew. Chem.* **2008**, *120* (44), 8522−8524.
(14) Petroselli, M.; Chen, Y.-Q.; Rebek, J. J.; Yu, Y. Binding and reactivity in deep cavitands based on resorcin[4]arene. *Green Synth. Catal.* **2021**, *2* (2), 123−130.
(15) Hong, J.; Djernes, K. E.; Lee, I.; Hooley, R. J.; Zaera, F. Heterogeneous Catalyst for the Selective Oxidation of Unactivated Hydrocarbons Based on a Tethered Metal-Coordinated Cavitand. *ACS Catal.* **2013**, *3* (9), 2154−2157.
(16) Giri, A.; Sahoo, A.; Dutta, T. K.; Patra, A. Cavitand and Molecular Cage-Based Porous Organic Polymers. *ACS omega* **2020**, *5* (44), 28413−28424.
(17) Zhang, J.-N.; Xia, Y.-X.; Zhang, H.-J. Natural Cyclopeptides as Anticancer Agents in the Last 20 Years. *Int. J. Mol. Sci.* **2021**, *22* (8), No. 3973, DOI: 10.3390/ijms22083973.
(18) Tan, N.-H.; Zhou, J. Plant cyclopeptides. *Chem. Rev.* **2006**, *106* (3), 840−895.
(19) Ashton, P. R.; Königer, R.; Stoddart, J. F.; Alker, D.; Harding, V. D. Amino Acid Derivatives of β-Cyclodextrin. *J. Org. Chem.* **1996**, *61* (3), 903−908.
(20) Xu, L.; Xing, C.-Y.; Ke, D.; Chen, L.; Qiu, Z.-J.; Zeng, S.-L.; Li, B.-J.; Zhang, S. Amino-Functionalized β-Cyclodextrin to Construct Green Metal-Organic Framework Materials for CO2 Capture. *ACS Appl. Mater. Interfaces* **2020**, *12* (2), 3032−3041.
(21) Bergman, H. M.; Kiel, G. R.; Handford, R. C.; Liu, Y.; Tilley, T. D. Scalable, Divergent Synthesis of a High Aspect Ratio Carbon Nanobelt. *J. Am. Chem. Soc.* **2021**, *143* (23), 8619−8624.
(22) Lu, X.; Gopalakrishna, T. Y.; Han, Y.; Ni, Y.; Zou, Y.; Wu, J. Bowl-Shaped Carbon Nanobelts Showing Size-Dependent Properties and Selective Encapsulation of C70. *J. Am. Chem. Soc.* **2019**, *141* (14), 5934−5941.
(23) Xie, J.; Li, X.; Du, Z.; Liu, Y.; Zhu, K. C−H···S Hydrogen Bond Assisted Supramolecular Encapsulation of Fullerenes with Nanobelts. *CCS Chem.* **2022**, 958−970, DOI: 10.31635/ccschem.022.202202019.
(24) Asim, M. H.; Ijaz, M.; Rösch, A. C.; Bernkop-Schnürch, A. Thiolated cyclodextrins: New perspectives for old excipients. *Coord. Chem. Rev.* **2020**, *420*, No. 213433, DOI: 10.1016/j.ccr.2020.213433.
(25) Park, C.; Youn, H.; Kim, H.; Noh, T.; Kook, Y. H.; Oh, E. T.; Park, H. J.; Kim, C. Cyclodextrin-covered gold nanoparticles for targeted delivery of an anti-cancer drug. *J. Mater. Chem.* **2009**, *19* (16), 2310−2315, DOI: 10.1039/b816209c.
(26) Akhgari, F.; Fattahi, H.; Oskoei, Y. M. Recent advances in nanomaterial-based sensors for detection of trace nitroaromatic explosives. *Sens. Actuators, B* **2015**, *221*, 867−878.
(27) To, K. C.; Ben-Jaber, S.; Parkin, I. P. Recent Developments in the Field of Explosive Trace Detection. *ACS Nano* **2020**, *14* (9), 10804−10833.
(28) Schroeder, V.; Savagatrup, S.; He, M.; Lin, S.; Swager, T. M. Carbon Nanotube Chemical Sensors. *Chem. Rev.* **2019**, *119* (1), 599−663.
(29) Norizan, M. N.; Moklis, M. H.; Demon, S. Z. N.; Halim, N. A.; Samsuri, A.; Mohamad, I. S.; Knight, V. F.; Abdullah, N. Carbon nanotubes: functionalisation and their application in chemical sensors. *RSC Adv.* **2020**, *10* (71), 43704−43732, DOI: 10.1039/D0RA09438B.
(30) Ellis, J. E.; Star, A. Carbon Nanotube Based Gas Sensors toward Breath Analysis. *ChemPlusChem* **2016**, *81* (12), 1248−1265.
(31) Luo, S.-X. L.; Swager, T. M. Chemiresistive sensing with functionalized carbon nanotubes. *Nat. Rev. Methods Primers* **2023**, *3* (1), No. 73, DOI: 10.1038/s43586-023-00255-6.
(32) Cheung, K. Y.; Segawa, Y.; Itami, K. Synthetic Strategies of Carbon Nanobelts and Related Belt-Shaped Polycyclic Aromatic Hydrocarbons. *Chem. - Eur. J.* **2020**, *26* (65), 14791−14801.
(33) Li, Y.; Kono, H.; Maekawa, T.; Segawa, Y.; Yagi, A.; Itami, K. Chemical Synthesis of Carbon Nanorings and Nanobelts. *Acc. Mater. Res.* **2021**, *2* (8), 681−691.
(34) Haver, R.; Anderson, H. L. Synthesis and Properties of Porphyrin Nanotubes. *Helv. Chim. Acta* **2019**, *102* (1), No. e1800211.
(35) Hündgen, M.; Maier, K. A.; Höger, S.; Jester, S.-S. Supramolecular nanopatterns of H-shaped molecules. *Chem. Commun.* **2018**, *54* (75), 10558−10561.
(36) Meißner, S. A.; Eder, T.; Keller, T. J.; Hofmeister, D. A.; Spicher, S.; Jester, S.-S.; Vogelsang, J.; Grimme, S.; Lupton, J. M.; Höger, S. Nanoscale π-conjugated ladders. *Nat. Commun.* **2021**, *12* (1), No. 6614, DOI: 10.1038/s41467-021-26688-9.
(37) Höger, S. Shape-persistent macrocycles: from molecules to materials. *Chem. - Eur. J.* **2004**, *10* (6), 1320−1329.
(38) Zhang, W.; Moore, J. S. Shape-persistent macrocycles: structures and synthetic approaches from arylene and ethynylene building blocks. *Angew. Chem., Int. Ed.* **2006**, *45* (27), 4416−4439.
(39) Grave, C.; Schlüter, A. D. Shape-Persistent, Nano-Sized Macrocycles. *Eur. J. Org. Chem.* **2002**, *2002* (18), 3075−3098.
(40) Höger, S.; Bonrad, K. No Job Name. *J. Org. Chem.* **2000**, *65* (7), 2243−2245.
(41) Mössinger, D.; Chaudhuri, D.; Kudernac, T.; Lei, S.; Feyter, S. de.; Lupton, J. M.; Höger, S. Large all-hydrocarbon spoked wheels of high symmetry: modular synthesis, photophysical properties, and surface assembly. *J. Am. Chem. Soc.* **2010**, *132* (4), 1410−1423.
(42) Ciszek, J. W.; Tour, J. M. Synthesis of ladder polyaromatics as new molecular device candidates. *Tetrahedron Lett.* **2004**, *45* (13), 2801−2803.
(43) Estrada, L. A.; Neckers, D. C. Synthesis and photophysics of ambipolar fluoren-9-ylidene malononitrile derivatives. *J. Org. Chem.* **2009**, *74* (21), 8484−8487.
(44) Estrada, L. A.; Neckers, D. C. Synthesis and photophysics of dibenza,cphenazine derivatives. *Org. Lett.* **2011**, *13* (13), 3304−3307.
(45) Qin, T.; Zhou, G.; Scheiber, H.; Bauer, R. E.; Baumgarten, M.; Anson, C. E.; List, E. J. W.; Müllen, K. Polytriphenylene Dendrimers: A Unique Design for Blue-Light-Emitting Materials. *Angew. Chem.* **2008**, *120* (43), 8416−8420.
(46) Shirai, Y.; Osgood, A. J.; Zhao, Y.; Yao, Y.; Saudan, L.; Yang, H.; Yu-Hung, C.; Alemany, L. B.; Sasaki, T.; Morin, J.-F.; Guerrero, J. M.; Kelly, K. F.; Tour, J. M. Surface-rolling molecules. *J. Am. Chem. Soc.* **2006**, *128* (14), 4854−4864.
(47) Bannwarth, C.; Ehlert, S.; Grimme, S. GFN2-xTB-An Accurate and Broadly Parametrized Self-Consistent Tight-Binding Quantum Chemical Method with Multipole Electrostatics and Density-Dependent Dispersion Contributions. *J. Chem. Theory Comput.* **2019**, *15* (3), 1652−1671.
(48) Bannwarth, C.; Caldeweyher, E.; Ehlert, S.; Hansen, A.; Pracht, P.; Seibert, J.; Spicher, S.; Grimme, S. Extended tight-binding quantum chemistry methods. *WIREs Comput. Mol. Sci.* **2021**, *11* (2), No. e1493, DOI: 10.1002/wcms.1493.

(49) Semiempirical Extended Tight-Binding Program Package. https://github.com/grimme-lab/xtb (accessed November 06, 2022).
(50) Lei, S.-B.; Deng, K.; Yang, Y.-L.; Zeng, Q.-D.; Wang, C.; Ma, Z.; Wang, P.; Zhou, Y.; Fan, Q.-L.; Huang, W. Substituent Effects on Two-Dimensional Assembling and Chain Folding of Rigid-Rod Polymer Poly(p -phenyleneethynylene) Derivatives on the Solid/Liquid Interface. *Macromolecules* **2007**, *40* (13), 4552−4560.
(51) Jeschke, G.; Sajid, M.; Schulte, M.; Ramezanian, N.; Volkov, A.; Zimmermann, H.; Godt, A. Flexibility of shape-persistent molecular building blocks composed of p-phenylene and ethynylene units. *J. Am. Chem. Soc.* **2010**, *132* (29), 10107−10117.
(52) Hinderer, F.; May, R.; Jester, S.-S.; Höger, S. Monodisperse Oligo(p -phenylene−butadiynylene)s: GPC Conversion Factors and Self-Assembled Monolayers. *Macromolecules* **2016**, *49* (5), 1816−1821.
(53) Schweez, C.; Shushkov, P.; Grimme, S.; Höger, S. Synthesis and Dynamics of Nanosized Phenylene-Ethynylene-Butadiynylene Rotaxanes and the Role of Shape Persistence. *Angew. Chem., Int. Ed. Engl.* **2016**, *55* (10), 3328−3333.
(54) Wilhelm, P.; Schedlbauer, J.; Hinderer, F.; Hennen, D.; Höger, S.; Vogelsang, J.; Lupton, J. M. Molecular excitonic seesaws. *Proc. Natl. Acad. Sci. U.S.A.* **2018**, *115* (16), E3626−E3634.
(55) Giancarlo, L. C.; Flynn, G. W. Scanning tunneling and atomic force microscopy probes of self-assembled, physisorbed monolayers: peeking at the peaks. *Annu. Rev. Phys. Chem.* **1998**, *49*, 297−336.
(56) Groszek, A. J. Selective adsorption at graphite/hydrocarbon interfaces. *Proc. R. Soc. A: Math. Phys. Eng. Sci.* **1970**, *314* (1519), 473−498, DOI: 10.1098/rspa.1970.0019.
(57) McGonigal, G. C.; Bernhardt, R. H.; Thomson, D. J. Imaging alkane layers at the liquid/graphite interface with the scanning tunneling microscope. *Appl. Phys. Lett.* **1990**, *57* (1), 28−30.
(58) Rabe, J. P.; Buchholz, S. Commensurability and mobility in two-dimensional molecular patterns on graphite. *Science* **1991**, *253* (5018), 424−427.
(59) Yang, T.; Berber, S.; Liu, J.-F.; Miller, G. P.; Tománek, D. Self-assembly of long chain alkanes and their derivatives on graphite. *J. Chem. Phys.* **2008**, *128* (12), No. 124709.
(60) Ilan, B.; Florio, G. M.; Hybertsen, M. S.; Berne, B. J.; Flynn, G. W. Scanning tunneling microscopy images of alkane derivatives on graphite: role of electronic effects. *Nano Lett.* **2008**, *8* (10), 3160−3165.
(61) Rabe, J. P.; Buchholz, S.; Askadskaya, L. Scanning tunneling microscopy of chain-molecules at solid-fluid-interfaces. *Phys. Scr.* **1993**, *T49A*, 260−263.
(62) Wawkuschewski, A.; Cantow, H.-J.; Magonov, S. N.; Möller, M.; Liang, W.; Whangbo, M.-H. STM study of molecular order and defects in the layers of cycloalkanes (CH2)48 and (CH2)72 adsorbed on graphite. *Adv. Mater.* **1993**, *5* (11), 821−826.
(63) Hibino, M.; Tsuchiya, H. Coexistence of Alkylated Sulfide Molecules along Two Orthogonal Directions of Graphite Lattice. *J. Phys. Chem. C* **2014**, *118* (3), 1484−1491.
(64) Keller, T. J.; Sterzenbach, C.; Bahr, J.; Schneiders, T. L.; Bursch, M.; Kohn, J.; Eder, T.; Lupton, J. M.; Grimme, S.; Höger, S.; Jester, S.-S. Nanopatterns of molecular spoked wheels as giant homologues of benzene tricarboxylic acids. *Chem. Sci.* **2021**, *12* (27), 9352−9358.
(65) Stine, R.; Mulvaney, S. P.; Robinson, J. T.; Tamanaha, C. R.; Sheehan, P. E. Fabrication, optimization, and use of graphene field effect sensors. *Anal. Chem.* **2013**, *85* (2), 509−521.
(66) Niu, L.; Luo, Y.; Li, Z. A highly selective chemical gas sensor based on functionalization of multi-walled carbon nanotubes with poly(ethylene glycol). *Sens. Actuators, B* **2007**, *126* (2), 361−367.
(67) Wang, F.; Yang, Y.; Swager, T. M. Molecular recognition for high selectivity in carbon nanotube/polythiophene chemiresistors. *Angew. Chem., Int. Ed. Engl.* **2008**, *47* (44), 8394−8396.
(68) Rao, A. M.; Eklund, P. C.; Bandow, S.; Thess, A.; Smalley, R. E. Evidence for charge transfer in doped carbon nanotube bundles from Raman scattering. *Nature* **1997**, *388* (6639), 257−259.
(69) Moore, D. S. Instrumentation for trace detection of high explosives. *Rev. Sci. Instrum.* **2004**, *75* (8), 2499−2512.
(70) Luo, S.-X. L.; Lin, C.-J.; Ku, K. H.; Yoshinaga, K.; Swager, T. M. Pentiptycene Polymer/Single-Walled Carbon Nanotube Complexes: Applications in Benzene, Toluene, and o-Xylene Detection. *ACS Nano* **2020**, *14* (6), 7297−7307.
(71) Chen, P.-C.; Sukcharoenchoke, S.; Ryu, K.; de Arco, L. G.; Badmaev, A.; Wang, C.; Zhou, C. 2,4,6-Trinitrotoluene (TNT) chemical sensing based on aligned single-walled carbon nanotubes and ZnO nanowires. *Adv. Mater.* **2010**, *22* (17), 1900−1904, DOI: 10.1002/adma.200904005.
(72) Han, T.; Nag, A.; Chandra Mukhopadhyay, S.; Xu, Y. Carbon nanotubes and its gas-sensing applications: A review. *Sens. Actuators, A* **2019**, *291*, 107−143.
(73) Kumar, D.; Jha, P.; Chouksey, A.; Tandon, R. P.; Chaudhury, P. K.; Rawat, J. S. Flexible single walled nanotube based chemical sensor for 2,4-dinitrotoluene sensing. *J. Mater. Sci.: Mater. Electron.* **2018**, *29* (8), 6200−6205.
(74) *NSTI-Nanotech 2013*, Technical proceedings of the 2013 NSTI Nanotechnology Conference and Expo, Laudon, M.; Romanowicz, B., Eds.; CRC Press, 2013.
(75) Park, M.; Tsai, S.-L.; Chen, W. Microbial biosensors: engineered microorganisms as the sensing machinery. *Sensors* **2013**, *13* (5), 5777−5795.
(76) Zhang, Y.; Xu, M.; Bunes, B. R.; Wu, N.; Gross, D. E.; Moore, J. S.; Zang, L. Oligomer-coated carbon nanotube chemiresistive sensors for selective detection of nitroaromatic explosives. *ACS Appl. Mater. Interfaces* **2015**, *7* (14), 7471−7475.
(77) Wei, L.; Lu, D.; Wang, J.; Wei, H.; Zhao, J.; Geng, H.; Zhang, Y. Highly sensitive detection of trinitrotoluene in water by chemiresistive sensor based on noncovalently amino functionalized single-walled carbon nanotube. *Sens. Actuators, B* **2014**, *190*, 529−534.
(78) Cumming, C. J.; Aker, C.; Fisher, M.; Fok, M.; La Grone, M. J.; Reust, D.; Rockley, M. G.; Swager, T. M.; Towers, E.; Williams, V. Using novel fluorescent polymers as sensory materials for above-ground sensing of chemical signature compounds emanating from buried landmines. *IEEE Trans. Geosci. Remote Sens.* **2001**, *39* (6), 1119−1128.

https://doi.org/10.1021/jacs.3c08131
J. Am. Chem. Soc. 2024, 146, 2986−2996